Far-Infrared Absorption of $La_{1-x}Ca_xMnO_{3-y}$ at High Pressure

A. Sacchetti,[1] M. Cestelli Guidi,[2] E. Arcangeletti,[1] A. Nucara,[1] P. Calvani,[1] M. Piccinini,[2] A. Marcelli,[2] and P. Postorino[1]

[1]"Coherentia" CNR-INFM and Dipartimento di Fisica, Università di Roma La Sapienza, Piazzale Aldo Moro 2, I-00185 Roma, Italy

[2]Laboratori Nazionali di Frascati—INFN, Via E. Fermi 40, 00044 Frascati, Italy

(Received 3 August 2005; published 24 January 2006)

The first far-infrared absorption spectra of manganite samples at pressures P up to 10 GPa were obtained on $La_{1-x}Ca_xMnO_{3-y}$ by use of synchrotron radiation. For $x = 0.25$ and 0.20 ($y = 0$), P promotes partial metallization at room temperature through a strong reduction of the insulating gap. An $x = 0.20$ sample with $y = 0.08$ does not show any charge delocalization effect up to 10 GPa. An Urbach-like model of disordered Jahn-Teller wells is shown to well fit the far-infrared band edge and allows one to obtain a reliable pressure dependence of the energy gap.

DOI: 10.1103/PhysRevLett.96.035503 PACS numbers: 63.20.Kr, 62.50.+p, 71.30.+h, 78.30.−j

The pressure-driven insulator-to-metal transition (IMT) is one of the most intriguing phenomena exhibited by condensed matter. The volume compression has usually the effect of both symmetrizing the crystal structure and increasing the overlap among the electronic clouds of the elemental units (ions and/or molecules) leading to a delocalization of the outer electrons. Despite the above oversimplified picture, the actual path followed by an insulating system towards metallization is peculiar and usually complex since volume compression can also modify the balance among microscopic interactions. High pressure can be an ideal tool to gain a deeper knowledge when dealing with complex systems where different interactions are simultaneously at work. This is the case of $La_{1-x}Ca_xMnO_3$ manganites within the $0.20 < x < 0.50$ doping range [1], which undergo a transition from a high-temperature, paramagnetic, insulating phase to a ferromagnetic metallic phase at T_{IM}, which apparently coincides with the Curie temperature T_c. It is now widely accepted that the IMT originates from a competition between the ferromagnetic Mn ordering induced by itinerant holes through the double-exchange (DE) mechanism and an effective electron-phonon coupling (EPC) due to the Jahn-Teller (JT) distortion of the $Mn^{+3}O_6$ octahedra [2,3]. The latter, removing the degeneracy of the outer Mn d orbital with e_g symmetry, tends to localize the carrier through polaronic self-trapping.

The IMT temperature T_{IM} is expected to be proportional to the effective e_g orbital bandwidth, which in turn is usually factorized into a bare structural term W_0 and a narrowing factor $\chi < 1$, which depends on the EPC [4,5]. In principle, the application of external pressure should monotonically increase T_{IM}, as it: (i) increases W_0 by increasing the superposition of the Mn, O orbitals; (ii) increases χ by reducing the EPC through a symmetrization of the octahedra [4]. At variance with this prediction, in $La_{0.75}Ca_{0.25}MnO_3$ [6,7] T_{IM} (P) increases linearly only up to $P \approx 3$ GPa and seems to approach an asymptotic value around room temperature beyond $P \approx 6$ GPa. This unexpected high-pressure behavior has been observed also in other manganites [8,9] and can be explained as a competition between mechanisms (i) and (ii) plus a pressure-enhanced localization due to superexchange, antiferromagnetic interaction [8,10]. As a final remark, we observe that the above picture may become even more complex if the suggestion for a phase separation regime [11], where the metallic phase would be established by percolation paths through metallic domains dispersed in an insulating matrix [11,12], is let in.

As the charge carriers are described in terms of JT polarons, their behavior can be efficiently studied through their optical absorption. The localized small polarons of the insulating phase will produce strong bands in the mid and near infrared peaked at twice the self-trapping energy [13], whose low-energy edge marks the insulating gap E_g. The charge delocalization process which leads to the IMT will be observed through an increase of the spectral weight on the low-frequency side of the polaronic band, an increased phonon shielding, and eventually a closing of the gap ($E_g \rightarrow 0$). Direct optical observations of this process have been reported by approaching the metallization through temperature variations [6,14].

Here, we first report on the observation of a far-infrared (FIR) gap filling in a manganite, obtained by varying the pressure at constant (room) temperature. To this purpose, a membrane diamond anvil cell (DAC) equipped with II A diamonds 800 μm culet was used. The gaskets were made of a 250 μm thick steel foil with a sample chamber of 300 μm diameter and 40 to 50 μm height under working conditions. Collection of high quality FIR data through two diamonds and with such a small sample area is not possible by use of conventional sources. We then illuminated the DAC by the synchrotron radiation provided by the beam line SINBAD which extracts FIR radiation from a bending magnet of the 0.51 GeV double ring DAΦNE at LNF-INFN Frascati [15]. The intensity $I(\omega)$ transmitted by the full DAC cell ($\omega = 200$ cm^{-1}) was by a factor of 40 higher than for the mercury lamp of the interferometer,

and the signal-to-noise ratio increased, correspondingly [16]. The samples were three $La_{1-x}Ca_xMnO_{3-y}$ polycrystalline manganites [17] with different Ca concentration and oxygen stoichiometry. This allowed one to obtain different effective doping values $x_{\text{eff}} \sim x - 2y$, (see Table I). At ambient pressure, the resistivity of the stoichiometric samples LC25S and LC20S showed IMT at $T_{\text{IM}} = 220$ and 200 K, respectively, whereas the oxigen-deficent LC20D did not show any metallic phase at low temperature. Very thin sample slabs (see Table I), obtained by pressing finely milled sample powder between the diamond anvils, have been placed in the gasket hole using petroleum jelly as a pressure transmitting medium [18]. We verified that no chemical reaction occurred between the jelly and the sample, by comparing the ambient pressure spectra collected before and after each pressure run. Pressure was measured *in situ* by the usual ruby fluorescence method [19] before and after each data collection. Visual inspection of the loaded samples revealed the presence of fractures over a small fraction η of total slab area. The η values reported in Table I were estimated from microscope pictures.

We verified once and for all that the transmittance spectrum of the DAC, when filled with the hydrostatic medium only, was actually flat vs ω and simply proportional to the intensity $I_0(\omega)$ transmitted by a pinhole of the same aperture, in the frequency region of interest (100–700 cm^{-1}). Therefore, the *measured* optical density, $\text{OD}_M(\omega)$, was obtained at each pressure using the intensities transmitted by the DAC + sample, $I(\omega)$, and by a 300 μm diameter pinhole, i.e., $\text{OD}_M(\omega) = \ln[I_0(\omega)/I(\omega)]$. Data were then corrected for the variation with time of the current in the synchrotron source. This procedure, although affecting the absolute values of the optical density by a constant, enables a quantitative comparison among the $\text{OD}_M(\omega)$ obtained for a given sample at different pressures, strongly simplifies the measurement procedure, and allows us to account for possible fluctuations of the synchrotron source.

It is worthwhile to notice that although η is small (see Table I), it can significantly affect high values of $\text{OD}_M(\omega)$. By neglecting diffraction effects, which are cancelled by the random shape of the fractures, if a fraction η of the sample surface transmits $I_0(\omega)$, the total transmitted intensity can be written as

$$I(\omega) = I_0(\omega)[(1 - \eta)\exp(-\text{OD}_t(\omega)) + \eta] \quad (1)$$

TABLE I. Ca doping x, effective charge doping x_{eff}, slab thickness d, and the percentage of fractures η in the sample area, for the three samples.

Sample		x	x_{eff}	d (μm)	η
$La_{0.75}Ca_{0.25}MnO_3$	(LC25S)	0.25	0.25	5	4%
$La_{0.80}Ca_{0.20}MnO_3$	(LC20S)	0.20	0.20	4	2%
$La_{0.80}Ca_{0.20}MnO_{2.92}$	(LC20D)	0.20	0.04	4	2%

where $\text{OD}_t(\omega)$ is the *true* optical density of the sample. The *measured* $\text{OD}_M(\omega)$ can be thus obtained by

$$\text{OD}_M(\omega) = -\ln[(1 - \eta)\exp(-\text{OD}_t(\omega)) + \eta]. \quad (2)$$

It is evident from Eq. (2) that $\text{OD}_M(\omega)$ cannot exceed $-\ln(\eta)$ which represents the saturation level of our measurements. The $\text{OD}_M(\omega)$ are shown in Fig. 1 for the three samples at different pressures. Three main phonon bands are apparent in all samples at ambient pressure. From high to low energy they are ascribed to the asymmetric octahedral stretching (at about 590 cm^{-1}), to the corresponding bending (380 cm^{-1}), and to an external mode of the rare earth (180 cm^{-1}) [20,21]. A remarkable pressure-induced hardening is observed only for the octahedral stretching mode. The high quality of the data in Fig. 1 is shown by the splitting in the central peak, induced by strong doping, and previously observed in a single crystal with $x = 0.33$ at ambient pressure [20]. An additional vibrational line is detected at $\sim$250 cm^{-1} and, in LC20S, at $\sim$320 cm^{-1}. Similar features observed in most perovskites at high doping, when polaronic effects are present, are probably related to the local distortion [13]. All those phonon structures are superimposed on the tail of a mid-infrared band, whose spectral weight decreases as the metallic character

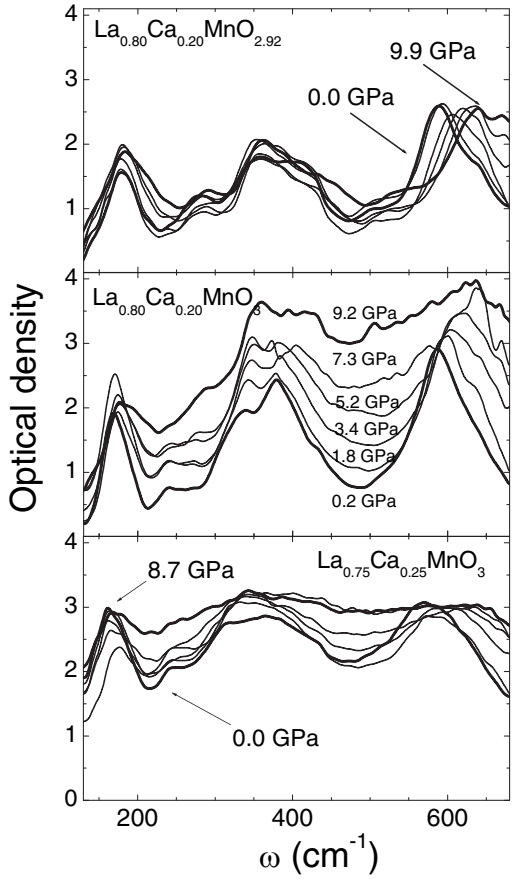

FIG. 1. Optical densities of the three $La_{1-x}Ca_xMnO_{3-y}$ samples at different pressure. Thick lines show the lowest and the highest working pressure.

of the sample decreases from LC25S to LC20S, to LC20D. A strong pressure dependence of the polaronic contribution is also apparent only in LC20S and LC25S, as well as a smearing of the phonon structures at the highest pressures. The former effect can be ascribed to a pressure-induced filling of the polaronic energy gap, the latter one to the partial screening of the phonon lines on approaching the metallic phase [6]. We point out that pressure appears to be ineffective in filling the gap of the LC20D sample, which preliminary ambient pressure measurements show to be around 700 cm^{-1} and, consistently with the absence of a metallic phase, almost temperature independent.

We finally notice that although saturation effects are clearly present in the spectra of the thickest LC25S, the polaronic contribution lies well below the saturation level at all pressures. The good data quality in Fig. 1 allows for detailed fits. We used a standard linear combination of damped harmonic oscillators to refine the phonon structures, and a model borrowed from semiconductor physics to fit the polaronic band edge. Therein, the effect of disorder on the crystal periodic potential is modeled by introducing a Gaussian distribution of the potential wells depth in a standard Kronig-Penney potential. This results in adding an exponential tail (Urbach tail) within the gap between the valence and the conduction band [22,23]. In the polaronic scenario of manganites, we assume that the Jahn-Teller potential wells, where the charge-carriers self-trap, have a similar Gaussian distribution. In close similarity with semiconductors, we expect that the optical density in the proximity of the gap is proportional to:

$$\begin{cases} A(\omega - \omega_g)^{1/2} & \omega > \omega_0 \\ B\exp(\omega/\Gamma) & \omega < \omega_0 \end{cases},$$

where the usual power law is replaced by the exponential (Urbach tail [23]) at low frequency. The continuity constraint at ω_0 on both the above functions and their first derivatives introduces two new equations linking the five parameters A, ω_g, B, Γ, and ω_0, thus reducing the number of independent parameters to three. We chose the band amplitude A, the energy gap ω_g, and Γ as free fitting parameters. Equation (2) has been also included in the fitting routine to account for the saturation effects. Two examples of best fits to the experimental data are shown in Fig. 2 for LC20S and LC20D at intermediate pressures. It is worth noting that both samples exhibit very similar phonon spectra, while the polaronic band is observed in the LC20S sample only. The results obtained for the phonon contributions, not discussed here, are consistent with those obtained in previous Raman experiments under pressure [24]. All the phonon bands of each sample show an almost linear pressure-induced frequency hardening, rather weak for the external and bending modes, much stronger for the stretching modes (about 6 cm^{-1}/GPa). The most

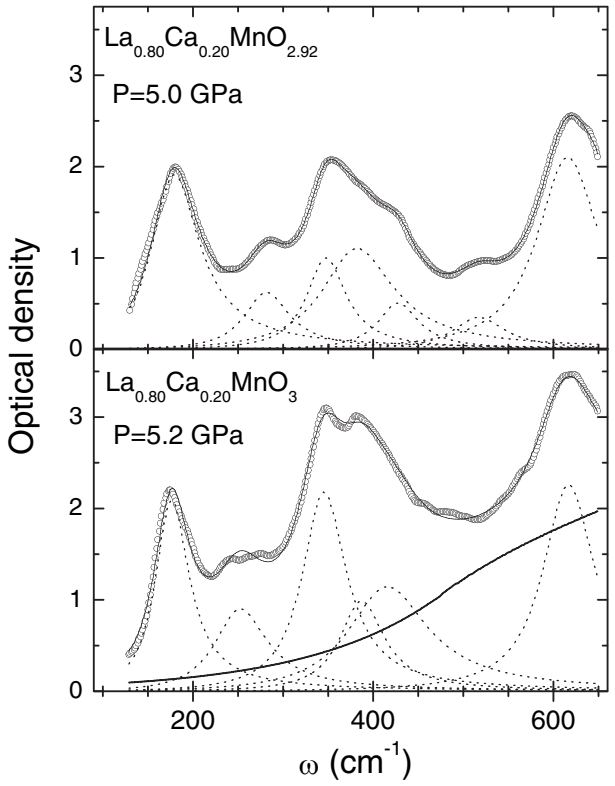

FIG. 2. Optical densities of LC20S and LC20D samples at $P \sim 5$ GPa (open circles) compared with the best fit curves (solid lines). The phonon contributions (dotted lines) are separately shown. The band edge (thick line) is also shown for the LC20S sample.

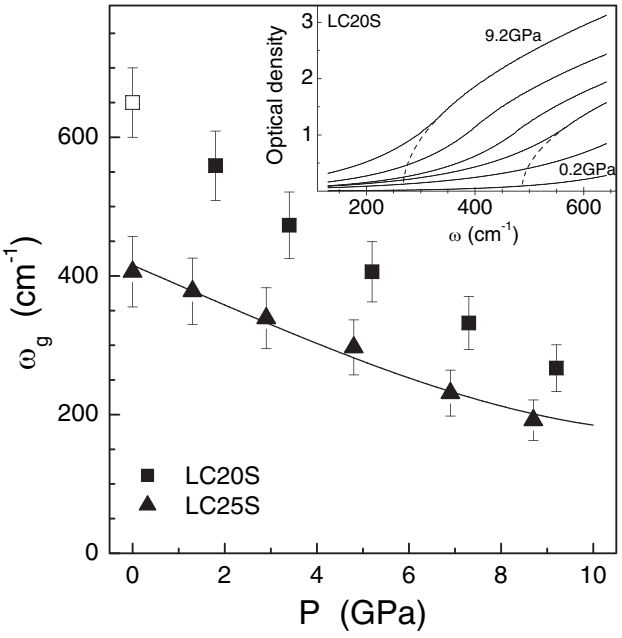

FIG. 3. Pressure dependence of the optical gap ω_g of LC25S and LC20S. The LC20S gap at $P = 0$ is obtained from a preliminary mid-infrared absorption measurement (empty square). The solid line is the ω_g behavior obtained from Eq. (3) with $E_{JT} = 0.8$ eV. The inset shows a polaronic band as a function of pressure in the LC20S sample; dashed lines mark the gap at $P = 3.4$ GPa and $P = 9.2$ GPa.

interesting findings come out from the analysis of the polaronic band edge of both stoichiometric samples (LC25S and LC20S) where this band is apparent and show a remarkable pressure dependence. The best fit values for the Urbach parameter Γ, which is directly related to the extent of disorder, are about 140 cm^{-1} and 240 cm^{-1} for LC20S and LC25S (i.e., of the same order of magnitude of those typical of several semiconductors [23]) and actually pressure independent. On the basis of the Urbach model, Γ is directly related to the variation of the potential well depth around an average value, not to the average value itself. The present results thus show that pressure does not affect disorder, namely, the distribution of the polaron binding energies. This suggests that disorder is mainly chemical, i.e., due to the random distribution of dopant ions.

The inset of Fig. 3 shows how the gap and the Urbach tail, as obtained from the fit to the LC20S absorption, change with pressure. For increasing P, the polaron spectral weight increases and the gap (see dashed lines) tends to close up. The pressure dependence of the band gap ω_g is shown in Fig. 3 for both samples which undergo the metallization process at room temperature.

Under simple assumptions, a relation among the energy gap value $E_g = hc\omega_g$, the JT energy E_{JT}, and the bare bandwidth W_0, can be written [25] as

$$E_g(P) = E_{JT}/2 - W_0(P). \quad (3)$$

Since $W_0(P)$ can be derived using structural parameters at high pressure [4] available for the LC25S sample [26], the present $E_g(P)$ data allow an estimate of E_{JT}. The line shown in Fig. 3 has been obtained from Eq. (3) with $E_{JT} = 0.8$ eV, in good agreement with previous experimental [25] and theoretical estimates for $La_{1-x}Ca_xMnO_3$ [27]. This further confirms the reliability of the model here first employed.

Although the band gap closure is a clear indication of the increased metallic character of the systems under pressure, a direct comparison between T_{IM} (P) and ω_g (P) is not straightforward. If we focus on LC25S, also investigated in Ref. [7], we can notice that around 9 GPa the value of T_{IM} is lower but quite close to 300 K [7], whereas the energy gap ω_g, although remarkably reduced, is still open ($\omega_g \sim 200$ cm^{-1}) and a crude linear extrapolation shows a room temperature band gap closure ($\omega_g = 0$) at a pressure higher than 15 GPa. One should also consider that $\omega_g(P)$ is an absolute, and bulk quantity, whereas the procedure in Ref. [7] may be sensitive to percolation paths through small metallic domains, as the good agreement between the estimate of T_{IM} from transport measurements and that from spectroscopy [6,14] points out. This behavior might be explained within a phase separation scenario where the majority of the sample remains in the insulating phase, whereas a metallic behavior would be established by percolation paths through small metallic domains [11,12].

In conclusion, we have here reported the first high-pressure measurements on a manganite in the far infrared, which were made possible by the use of infrared synchrotron radiation. The three $La_{1-x}Ca_xMnO_{3-y}$ samples we measured show a similar pressure dependence of the phonon spectrum, whereas only the two with a metallic ground state at ambient pressure ($T_{IM} \sim 200$ K) show a clear tendency to acquire a metallic character at room temperature under pressure. This is shown by a shielding of the phonon modes and a strong reduction of the insulating gap. This latter is well fitted at all pressures by a model borrowed from semiconductors and first applied to manganites, where the absorption in the gap region exhibits a $\omega^{1/2}$ decrease followed by an Urbach tail related to the random distribution of the JT self-trapping potential wells. As a consistency control on the model, we find for the JT splitting $E_{JT} = 0.8$ eV, in agreement with previous determinations.

We are gratefully indebted to T. Aselage, A. Kumar, and D. D. Sarma for providing the samples investigated.

[1] S.-W. Cheong and H. Y. Hwang, in *Colossal Magnetoresistance Oxides*, edited by Y. Tokura, Monographs in Condensed Matter Science (Gordon and Breach, Reading, U.K., 2000).
[2] A. J. Millis *et al.*, Phys. Rev. Lett. **77**, 175 (1996).
[3] A. J. Millis, Nature (London) **392**, 147 (1998).
[4] V. Laukhin *et al.*, Phys. Rev. B **56**, R10 009 (1997).
[5] H. Roder *et al.*, Phys. Rev. Lett. **76**, 1356 (1996).
[6] A. Congeduti *et al.*, Phys. Rev. B **63**, 184410 (2001).
[7] P. Postorino *et al.*, Phys. Rev. Lett. **91**, 175501 (2003).
[8] C. Cui and T. A. Tyson, Appl. Phys. Lett. **83**, 2856 (2003).
[9] C. Cui *et al.*, Phys. Rev. B **67**, 104107 (2003).
[10] P. Postorino *et al.*, Phys. Status Solidi B **241**, 3381 (2004).
[11] M. Fath *et al.*, Science **285**, 1540 (1999).
[12] E. Dagotto *et al.*, Phys. Rep. **344**, 1 (2001).
[13] P. Calvani, Riv. Nuovo Cimento **24**, 1 (2001).
[14] Y. Okimoto *et al.*, Phys. Rev. B **55**, 4206 (1997).
[15] E. Burattini *et al.*, Nucl. Instrum. Methods Phys. Res., Sect. A **347**, 308 (1994).
[16] M. Cestelli Guidi *et al.*, J. Opt. Soc. Am. A **22**, 2810 (2005).
[17] A. Nucara *et al.*, Phys. Rev. B **68**, 174432 (2003).
[18] B. Chen *et al.*, Phys. Rev. B **64**, 214111 (2001).
[19] H. K. Mao *et al.*, J. Appl. Phys. **49**, 3276 (1978).
[20] A. V. Boris *et al.*, Phys. Rev. B **59**, R697 (1999).
[21] K. H. Kim *et al.*, Phys. Rev. Lett. **77**, 1877 (1996).
[22] N. Bacalis *et al.*, Phys. Rev. B **37**, 2714 (1988).
[23] N. F. Mott and E. A. Davies, *Electronic Processes in Non-Crystalline Materials* (Clarendon, Oxford, 1971).
[24] A. Congeduti *et al.*, Phys. Rev. Lett. **86**, 1251 (2001).
[25] B. Lorenz *et al.*, Phys. Rev. B **63**, 144405 (2001), and references therein.
[26] C. Meneghini *et al.*, Phys. Rev. B**65**, 012111 (2002).
[27] A. J. Millis, Phys. Rev. B **53**, 8434 (1996).